

# Offset between stellar spiral arms and gas arms of the Milky Way

L. G. Hou<sup>\*</sup> and J. L. Han

*National Astronomical Observatories, Chinese Academy of Sciences, 20A DaTun Road, ChaoYang District, Beijing 100012, PR China*

Accepted 2015 ... Received 2015 ...

## ABSTRACT

Spiral arms shown by different components may not be spatially coincident, which can constrain formation mechanisms of spiral structure in a galaxy. We reassess the spiral arm tangency directions in the Milky Way through identifying the bump features in the longitude plots of survey data for infrared stars, radio recombination lines (RRLs), star formation sites, CO, high density regions in clouds, and HI. The bump peaks are taken as indications for arm tangencies, which are close to the real density peaks near the spiral arm tangency point but often have  $\sim 1^\circ$  offset to the interior of spiral arms. The arm tangencies identified from the longitudes plots for RRLs, HII regions, methanol masers, CO, high density gas regions, and HI gas appear nearly the same Galactic longitude, and therefore there is no obvious offset for spiral arms traced by different gas components. However, we find obvious displacements of  $1.3^\circ - 5.8^\circ$  between gaseous bump peaks from the directions of the maximum density of old stars near the tangencies of the Scutum-Centaurus Arm, the northern part of the Near 3 kpc Arm, and maybe also the Sagittarius Arm. The offsets between the density peaks of gas and old stars for spiral arms are comparable with the arm widths, which is consistent with expectations for quasi-stationary density wave in our Galaxy.

**Key words:** Galaxy: disk — Galaxy: structure — Galaxy: kinematics and dynamics

## 1 INTRODUCTION

The formation and evolution of spiral arms in spiral galaxies is a fundamental problem in astronomy for more than 90 years (e.g., Hubble 1926; Lindblad 1927). Observationally, spiral galaxies can be classified into, for example by Elmegreen (1990), flocculent (e.g., NGC 4414), multi-armed (e.g., M 101), and grand design galaxies (e.g., M 51). The mechanisms for spiral formation (see Dobbs & Baba 2014, for a review) could be (1) quasi-stationary density wave theory (e.g., Lin & Shu 1964, 1966); (2) localized instabilities, perturbations, or noise induced kinematic spirals (e.g., Sellwood & Carlberg 1984); (3) dynamically tidal interactions (e.g., Toomre & Toomre 1972). It is difficult to identify which mechanism dominates spiral structure in a specific galaxy (e.g., Binney & Tremaine 2008). Careful comparisons of spiral features between observations and theories are necessary to distinguish these mechanisms (Foyle et al. 2011).

The quasi-stationary density wave theory (Roberts 1969) predicts a spatial offset of different arm components, e.g., old stars, star forming regions, molecular gas and atomic gas, due to possible delay in star formation from gas gathering (see Fig. 1). The other mechanisms do not predict the offset between the stellar spiral arms and gaseous arms (see, e.g., Dobbs & Baba 2014; Baba et al. 2015). Face-on spiral galaxies (e.g., M 51, M 81) are the ideal objects to test these mechanisms. Many observations have been made (e.g., Mathewson et al. 1972; Rots 1975; Tamburro et al. 2008;

Egusa et al. 2009; Foyle et al. 2011; Martínez-García & Puerari 2014), but different conclusions were made by different authors even from the high quality data of HI, CO, 24  $\mu$ m infrared and UV images of the same sample of galaxies, mainly because of large uncertainties in measuring the spiral arm properties (Dobbs & Baba 2014).

For the Milky Way Galaxy, the possible spatial offset of different spiral arm components is very difficult to measure and far from clear at present, mainly because the spiral pattern and positions of arms (e.g. Vallée 2008; Foster & Cooper 2010; Hou & Han 2014; Pettitt et al. 2014; Carraro 2015) have not been well determined. However, the directions of spiral arm tangencies in our Galaxy can be estimated (e.g., Benjamin 2009), which can be used to check the possible offset between different components of spiral arms (e.g., see Fig. 1).

Previously spiral arm tangencies have been identified from the Galactic plane surveys of HI (e.g., Burton & Shane 1970; Weaver 1970),  $^{12}\text{CO}$  (e.g., Sanders et al. 1985; Solomon et al. 1985; Dame et al. 1986; Grabelsky et al. 1987; Bronfman et al. 1988, 1989, 2000a,b; Dame & Thaddeus 2011),  $^{13}\text{CO}$  (e.g., Stark & Lee 2006), radio continuum emission at 408 MHz (e.g., Beuermann et al. 1985) and at 86 MHz (e.g., Mills et al. 1958), HII regions (e.g., Lockman 1979, 1989; Downes et al. 1980; Hou & Han 2014), near infrared emission (e.g., Hayakawa et al. 1981), far infrared dust emission (e.g., Bloemen et al. 1990; Drimmel 2000), far infrared cooling lines (Steiman-Cameron et al. 2010), 870  $\mu$ m continuum (Beuther et al. 2012), 6.7-GHz methanol masers (e.g., Caswell et al. 2011; Green et al. 2011, 2012), and

<sup>\*</sup> E-mail: lghou@nao.cas.cn

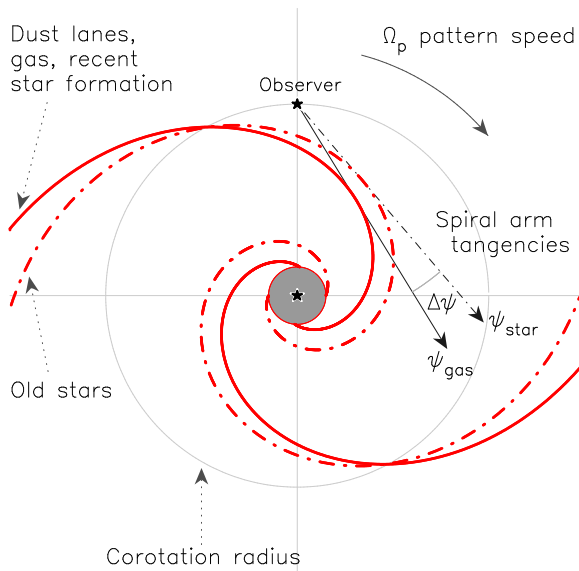


**Figure 1.** Schematic of the relative position between gas and old star components in spiral arms according to a quasi-stationary spiral structure in a face-on view [see also Fig. 1 of Martínez-García et al. (2009), Fig. 2 of Foyle et al. (2011), and Fig. 7 of Roberts (1969)]. Spiral arm tangencies for gas ( $\psi_{gas}$ ) and stars ( $\psi_{star}$ ) are shown by the density peaks near the tangency points of ideal spiral arms. Thus, the difference  $\Delta\psi = |\psi_{star} - \psi_{gas}|$  can be used to indicate the possible spatial offset of different components in spiral arms.

old stars (Churchwell et al. 2009) for the Scutum Arm, the Sagittarius Arm, the Carina Arm, the Centaurus Arm and the Norma Arm (e.g., see Table 1 of Englmaier & Gerhard 1999, and Vallée 2014a). In addition, the southern and northern tangencies for the Near 3 kpc Arm<sup>1</sup> have also been reported (e.g., Cohen & Davies 1976; Bania 1980; Dame & Thaddeus 2008). The directions of arm tangencies are regarded as important observational constraint on the Galaxy spiral arms (e.g., Burton 1971, 1973; Georgelin & Georgelin 1976; Englmaier & Gerhard 1999; Drimmel & Spergel 2001; Cordes & Lazio 2002; Russeil 2003; Churchwell et al. 2009; Hou et al. 2009; Hou & Han 2014; Vallée 2015). A detailed literature survey for spiral arm tangency directions can be found in Vallée (2014a).

The definitions of an arm tangency are often slightly different in literature, which makes direct comparison and even statistics difficult. For example, the arm tangency in Englmaier & Gerhard (1999, see their Sect. 4.6) is determined as the outer edge of a spiral arm where the velocity jump occurs. The arm tangency can be traced by discontinuities in the integrated CO emission, as mentioned by e.g. Bronfman et al. (2000a), Grabelsky et al. (1987), and Alvarez et al. (1990), or by the solid-body like kinematics in the rotation curve derived from CO survey (e.g., Luna et al. 2006). Spiral arms produce the deviations from the circular velocity, so

that the bumps in the rotation curves are anomalous velocities associated with streaming motion (see e.g. Burton & Shane 1970; Burton 1973; McClure-Griffiths & Dickey 2007). The arm tangency can also be identified from peak features (Drimmel 2000; Bronfman et al. 1989) or local maxima (Steiman-Cameron et al. 2010) in the longitude plot for integrated infrared emission or line intensities. Caswell et al. (2011) identified the Norma tangency as a dense concentration of methanol masers. The arm tangency can also be found by fitting the distributions of spiral tracers in the Galactic plane or by fitting the features in the longitude-velocity diagram with a spiral arm model (e.g., Hou & Han 2014). The derived arm tangency may be influenced by the position uncertainties of tracers. The derived directions of arm tangencies by different authors could be different as large as the half of arm width even from the same observational data.

There are some potential pitfalls on identifications of arm tangencies from observations. For example, velocity crowding, including the streaming motions (e.g., Burton 1973), and concentrations of individual clouds can result in the “bump” features in the longitude-velocity map or the number counts of objects. The clumps or cores of nearby clouds or star forming regions could be mistaken as the longitude concentrations of farther objects and then be misinterpreted as arm tangencies. In addition, gas observations for tangencies could be complicated by optical depth effects for some lines, such as the known self-absorption effect for the HI 21 cm line and CO line. Observations of small distant clouds can suffer beam dilution effect. To identify arm tangencies properly, the multi-wavelength survey data for different Galactic components should be considered together, because the problems discussed above may present in one or two datasets, but not in all datasets.

The spiral arms traced by old stars and molecular gas in our Milky Way are believed to be spatially coincident (e.g., Vallée 2014a). A spatial separation ( $\sim 100$  pc – 300 pc) between different arm tracers, e.g.,  $^{12}\text{CO}$ ,  $^{13}\text{CO}$ , HI gas, cold dust, methanol masers, hot dust, was recently suggested by Vallée (2014b), based on the statistics of arm tangency direction values in literature without considering possible different definitions. To show the possible offsets between spiral arms traced by different Galactic components, i.e., old stars, ionized gas, molecular gas, atomic gas, we reassess the spiral arm tangencies by using survey data in literature for different Galactic components.

## 2 SURVEY DATA FOR DIFFERENT GALACTIC COMPONENTS

### 2.1 Stellar component

Since the spiral structure traced by the stellar component were obtained by using the COBE survey (Drimmel 2000; Drimmel & Spergel 2001), data quality of two following surveys<sup>2</sup> has been improved significantly in the resolution and sensitivity with a greatly reduced extinction:

1) Two Micron All Sky Survey (2MASS, Skrutskie et al.

<sup>1</sup> The identification of the “3 kpc Arm” dates back to 1960s (e.g., van Woerden et al. 1957; Oort et al. 1958). There still are some debates on its nature (Green et al. 2011), which could be an expanding ring-like structure (e.g., van der Kruit 1971; Cohen & Davies 1976; Sevenster 1999), non-expanding resonance feature, or elliptical streamlines (e.g., Peters 1975), or spiral arms (e.g., Fux 1999; Bissantz et al. 2003). Two tangencies are observed for this structure in the inner Galaxy regardless of its nature. In this work, we take the name “3 kpc Arm” when referring to the feature.

<sup>2</sup> In fact, the Wide-field Infrared Survey Explorer (WISE, Wright et al. 2010) also finished an all sky survey at 3.4  $\mu\text{m}$ , 4.6  $\mu\text{m}$ , 12  $\mu\text{m}$ , and 22  $\mu\text{m}$ . The WISE data have a Point Spread Function of 6'' – 12'' in the 3  $\mu\text{m}$  to 24  $\mu\text{m}$  bands, and suffer from confusion near the Galactic midplane, hence, are not used in this work for distributions of old stars. While HII regions used in this paper were identified from WISE data (Anderson et al. 2014), see Sect. 2.2.

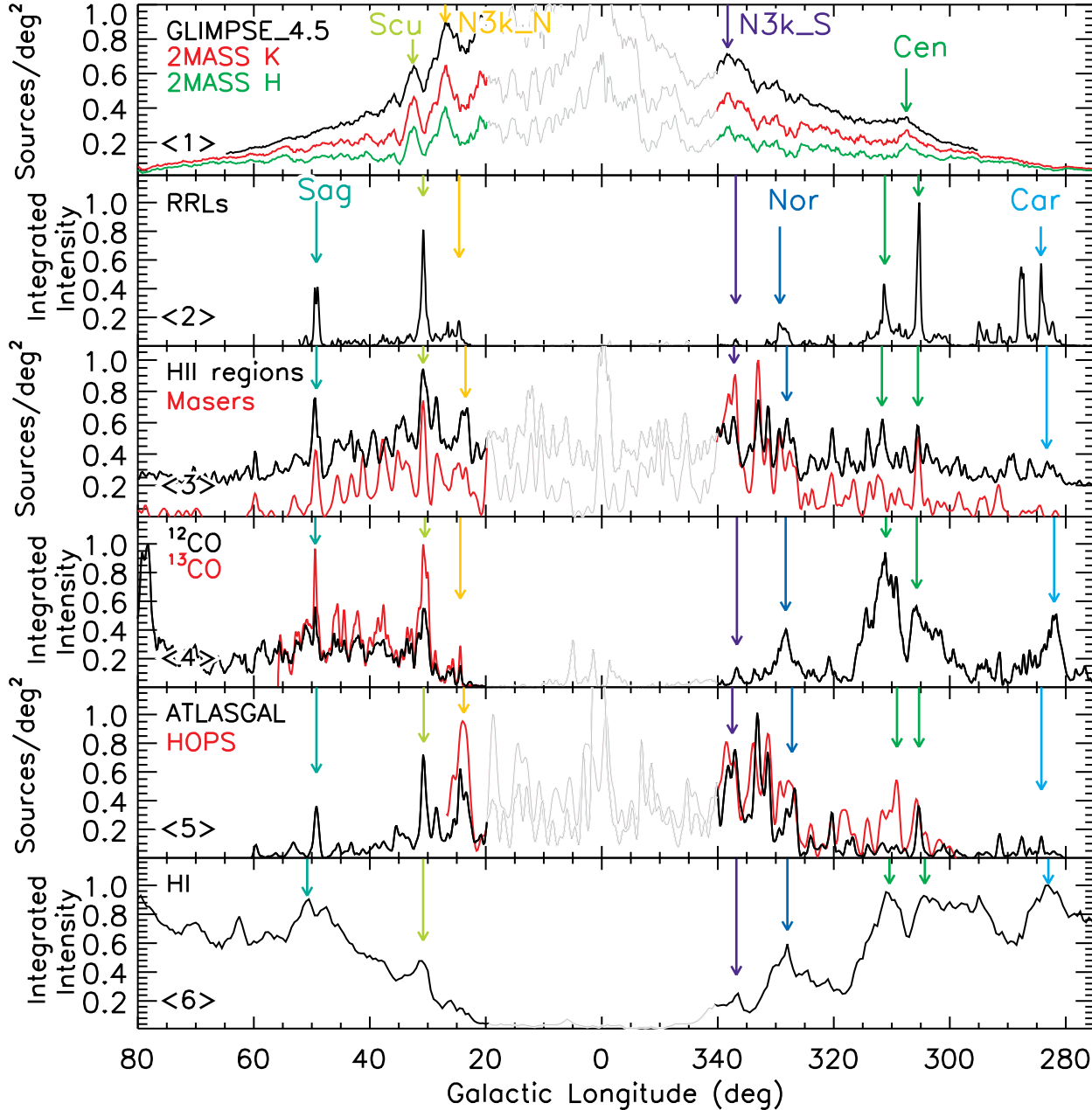


**Figure 2.** Surface density of old stars as a function of the Galactic longitude deduced from the survey data of GLIMPSE 4.5  $\mu\text{m}$  (black), 2MASS  $K_s$  band (red), 2MASS  $H$  band (green) is shown in *panel <1>*. The integrated intensity of the 1.4 GHz RRLs over the velocity range of  $\pm 15 \text{ km s}^{-1}$  from the tangency point velocity of a given direction is plotted against the Galactic longitude in *panel <2>*. The surface densities of HII regions (black) and 6.7-GHz methanol masers (red) are shown in *panel <3>*. The integrated intensity for molecular gas  $^{12}\text{CO}(1-0)$  (black) and  $^{13}\text{CO}(1-0)$  (red), again over  $\pm 15 \text{ km s}^{-1}$ , are plotted in *panel <4>* and *panel <5>*, respectively. The surface density for dense cores of molecular clouds detected from the ATLASGAL (black) and the HOPS (red) are plotted in *panel <5>*. Peaks for spiral arm tangency directions are indicated by arrows with different colors. The complex features in the regions close to the Galactic center direction ( $20^\circ > l > 340^\circ$ ) are not the scope of this article and plotted as gray lines. See text for references for the survey data, and for discussions for the identifications of spiral arm tangencies.

2006) observed almost the entire celestial sphere in three near-infrared bands, i.e.,  $J$  (1.25  $\mu\text{m}$ ),  $H$  (1.65  $\mu\text{m}$ ) and  $K_s$  (2.16  $\mu\text{m}$ ), produced a point source catalog containing 470, 992, 970 sources. The sensitivity ( $S/N = 10$ ) is 15.8 mag, 15.1 mag, and 14.3 mag for the  $J$ ,  $H$ , and  $K_s$  bands, respectively.

2) *Spitzer*/GLIMPSE (Galactic Legacy Infrared Midplane Extraordinaire) is a survey of the inner Galactic plane with the *Spitzer* space telescope in four mid-infrared bands, i.e., 3.6  $\mu\text{m}$ , 4.5  $\mu\text{m}$ ,

5.8  $\mu\text{m}$  and 8  $\mu\text{m}$  (Benjamin et al. 2003), providing a  $3\sigma$  sensitivity for point sources as being 15.5 mag, 15.0 mag, 13.0 mag and 13.0 mag, respectively (Churchwell et al. 2009). The GLIMPSE has a comparable resolution of  $\sim 1''$  and a sensitivity of  $\sim 0.5 \text{ mJy}$  to the 2MASS but with a greatly reduced extinction (Benjamin 2008). We note that about 90% of all the GLIMPSE stars are red giants, and a good fraction of them appear to be the red-clump giants (Churchwell et al. 2009) which have a very narrow luminosity

function around an absolute magnitude  $M_K = -1.61 \pm 0.03$  mag with an Gaussian width of  $\sigma_K = 0.22 \pm 0.03$  mag (e.g., Alves 2000; Cabrera-Lavers et al. 2007).

The point sources detected by GLIMPSE and 2MASS within the Galactic latitude range of  $|b| < 1^\circ$  and the magnitude range of  $\Delta m = 6.5 - 12.5$  are used in this paper for determination of spiral arm tangencies traced by old stars<sup>3</sup>. Surface number density of stars (per deg<sup>2</sup>) is plotted against the Galactic longitude in the top panel of Fig. 2. We ignore the regions close to the Galactic center direction (e.g.,  $20^\circ > l > 340^\circ$ ) where the bump features may be the superposition of structure features in the Galactic bar(s), bulge, and spiral arms. We focus only on the longitude regions of  $20^\circ < l < 340^\circ$ , where our plots are consistent with the results given by Churchwell et al. (2009, see their Fig. 14), Benjamin (2009, see their Fig. 2) and also Drimmel (2000, see their Fig. 1). Four broad and prominent bumps can be identified, which are interpreted in this paper as indication of spiral arm tangencies for the Scutum Arm ( $l \sim 32^\circ$ ), the Centaurus Arm ( $l \sim 308^\circ$ ) and the northern and southern ends of the Near 3 kpc Arm ( $l \sim 27^\circ$  and  $l \sim 338^\circ$ ) though the stellar bump near  $l \sim 27^\circ$  can also be interpreted by an in-plane bar or a ring (see Sect. 1 of López-Corredoira et al. 2001). The peak of the bumps are related to the density maximum in stellar spiral arms (see Sect. 3.2).

## 2.2 Ionized gas and star formation sites

Ionized gas exists in the interstellar medium in general in three forms: individual HII regions, diffuse warm ionized gas, and hot ionized gas (Lequeux 2005; Ferrière 2001). Radio recombination lines are best tracers of ionized gas (Gordon & Sorooshenko 2009). However, the global properties of ionized gas in the Milky Way revealed by RRLs are not well explored yet (e.g., Thompson et al. 2014; Liu et al. 2013; Alves et al. 2015; Bühr et al. 2015). At present, the HIPASS survey of the Galactic plane (Alves et al. 2010, 2015) has the largest sky coverage for mapping the RRLs in the region of  $l = 196^\circ - 0^\circ - 52^\circ$  and  $|b| \leq 5^\circ$  at 1.4 GHz with a resolution of 14.4 arcmin, picking up the RRLs of H168 $\alpha$ , H167 $\alpha$  and H166 $\alpha$  with a rms noise per channel of about 2.8 mK.

In the panel <2> of Fig. 2, the RRL line intensity integrated over  $|b| < 2^\circ$  and a velocity range of  $\Delta V = [V_t - 15 \text{ km s}^{-1}, V_t + 15 \text{ km s}^{-1}]$  around the terminal velocity  $V_t$  is plotted against the Galactic longitude. The velocity range  $\Delta V$  is so chosen to include the gas around the tangencies but exclude the foreground and background RRL emission. The terminal velocity  $V_t$  is calculated with a flat rotation curve and the IAU standard circular orbital speed at the Sun,  $\Theta_0 = 220 \text{ km s}^{-1}$ . The influences of the adopted rotation curves,  $\Theta_0$ , and velocity range  $\Delta V$  will be tested and discussed in Sect. 3.1.

In the RRL plot, each spiral arm shows a corresponding distinct bump. The bumps indicate that ionized gas traced by H168 $\alpha$ , H167 $\alpha$  and H166 $\alpha$  are concentrated to spiral arms. The bump peaks indicate the density maximums of ionized gas in spiral arms (see Sect. 3.2) and hence are adopted as the “observed” arm tangencies

of ionized gas. Some weaker bumps in the plots may indicate some individual clouds or arm spurs/branches in the interarm regions. The significance of a bump is evaluated by the ratio of the bump peak value to the fluctuation  $\sigma$  which is estimated from the fitting residual outside the range of a tangency.

The Centaurus arm is intriguing to have two distinct RRL bumps near  $l \sim 311^\circ$  and  $l \sim 305^\circ$ , which are also shown in the CO and HI plots and coincident with the dips in the rotation curve of McClure-Griffiths & Dickey (2007, see their Fig. 8).

HII regions are the zones of ionized gas surrounding young massive stars or star clusters. They are primary tracer of spiral arms. HII regions can be detected from the whole Galactic disk without extinction, even as far as  $\sim 20$  kpc from the Sun (see Hou & Han 2014). The largest catalog of Galactic HII regions or candidates to date is recently given by Anderson et al. (2014), who identified HII regions according to the mid-infrared morphology in the WISE survey data. More than 8400 HII regions and candidates are identified, about 1500 of them were previously known. However, most of the HII regions do not have line velocity information.

The 6.7 GHz methanol masers are good tracers of the early evolutionary stage of massive stars. About 1000 Galactic methanol masers have been detected (e.g., Pestalozzi et al. 2005; Ellingsen 2007; Xu et al. 2008; Cyganowski et al. 2009; Green et al. 2009, 2010, 2012; Caswell et al. 2010, 2011; Fontani et al. 2010; Olmi et al. 2014; Sun et al. 2014; Breen et al. 2015). The catalog of 6.7-GHz methanol masers collected by Hou & Han (2014) from literature is used in this work.

The number density of HII regions and methanol masers is plotted against the Galactic longitude in the panel <3> of Fig. 2. However, the identification of spiral arm tangencies in the plot is not straightforward as the bump features are not so clear. The star formation sites are very clumpy in general, and some bumps may be related to arm spurs or arm branches or clumpies in some nearby individual clouds, not to the major gaseous spiral arms. In addition, no velocity constraints were made in the plot due to the lack of velocity information for most HII regions. Some bump features are probably related to the star formation sites in the Sagittarius-Carina Arm and/or Scutum-Centaurus Arm. It is clear that spiral arm tangencies can be well-identified by RRL, CO and HI velocity integrated plots, and then we check the coincident features in the number density plot for HII regions and methanol masers. The bumps near the tangency directions can be found for the northern part of the Near 3 kpc Arm ( $l \sim 24^\circ$ ), the Scutum Arm ( $l \sim 32^\circ$ ), the Sagittarius Arm ( $l \sim 50^\circ$ ), the Centaurus Arm ( $l \sim 306^\circ, 312^\circ$ ), the Norma Arm ( $l \sim 328^\circ$ ), and the southern part of the Near 3 kpc Arm ( $l \sim 337^\circ$ ), which we marked arrows in Fig. 2. These bump peaks indicate the dense concentration of HII regions and methanol masers in spiral arms, hence are taken as the “observed” arm tangencies for star formation sites. The density excesses near the northern tangency of the Near 3 kpc Arm ( $l \sim 24^\circ$ ) and near the Carina tangency ( $l \sim 282^\circ$ ) are not prominent with a significance of only  $0.6\sigma - 2.6\sigma$ .

## 2.3 Molecular gas and high density sites

Carbon monoxide (CO) is a tracer for molecular gas in galaxies. By far the most widely-used survey of Galactic <sup>12</sup>CO(1–0) was given by Dame et al. (2001), which covers the entire Galactic plane and extends at least six degrees in the Galactic latitude. The angular resolution is  $8.4' - 8.8'$ . The rms noise per channel is about 0.3 K. The velocity coverage is from  $-260 \text{ km s}^{-1}$  to  $+280 \text{ km s}^{-1}$  in the frame of the Local Standard of Rest (LSR).

<sup>3</sup> The GLIMPSE Point Source Catalog is truncated at 6.5 mag due to the detector nonlinearity for bright sources (e.g., see Fig. 3. of Benjamin et al. 2005). In the inner Galaxy ( $|l| < 40^\circ$ ), the GLIMPSE is confusion-limited at 13.3–13.6 mag (Churchwell et al. 2009). Following Benjamin et al. (2005) and Churchwell et al. (2009), we adopt 12.5 mag as the fainter limit for the GLIMPSE and 2MASS source plots in Fig 2. The influence of the magnitude range on the derived spiral arm tangencies is tested and discussed in Sect. 3.1.

Emission of  $^{13}\text{CO}(1-0)$  suffers less extinction than that of  $^{12}\text{CO}(1-0)$ , hence it is a better tracer of column density for the molecular gas. The Galactic Ring Survey (GRS, Jackson et al. 2006) of  $^{13}\text{CO}(1-0)$  covers the longitude range from  $18^\circ$  to  $55.7^\circ$  and the latitude range of  $|b| \leq 1^\circ$ . The angular resolution is about  $46''$  and the sampling is  $22''$ . The sensitivity is about  $0.4\text{ K}$ . The LSR velocity coverage is from  $-5\text{ km s}^{-1}$  to  $+135\text{ km s}^{-1}$ .

In the panel <4> of Fig. 2, the variation of CO intensity integrated over  $|b| < 2^\circ$  and a velocity range of  $\Delta V = [V_t - 15\text{ km s}^{-1}, V_t + 15\text{ km s}^{-1}]$  around the terminal velocity is plotted against the Galactic longitude (e.g., see also Grabelsky et al. 1987). We see that near every spiral arm tangency there is a corresponding bump in the CO plot. The bump peaks in the CO plot is related to the density maximums of molecular gas in spiral arms (see Sect. 3.2). Therefore molecular clouds are good tracers of spiral structure (e.g., Hou & Han 2014), and the spiral arm tangencies can be shown by molecular gas. We note that around the tangency direction of the Centaurus arm, there are two distinct peaks of CO intensity, stronger one near  $l \sim 312^\circ$  and a weaker one near  $l \sim 306^\circ$ .

High density regions of molecular gas comprise only  $\sim 7\%$  of the mass of molecular clouds (Battisti & Heyer 2014), but they are the birth place of massive stars or star clusters. The best way to unambiguously search for high density regions is to survey the optically thin emission of dust in the millimeter/submillimeter regime (Csengeri et al. 2014; Andre et al. 2000). There have been some impressive progress in recent years, e.g., the Bolocam Galactic Plane Survey (Rosolowsky et al. 2010; Aguirre et al. 2011; Ginsburg et al. 2013), the APEX Telescope Large Area Survey of the Galaxy (ATLASGAL, Contreras et al. 2013; Csengeri et al. 2014), and the *Herschel Space Observatory* survey (Hi-Gal, Molinari et al. 2010a,b). The ATLASGAL at  $870\text{ }\mu\text{m}$  has been finished and cover a large portion of the inner Galactic plane ( $-60^\circ \leq l \leq +60^\circ$ , and  $-1.5^\circ \leq b \leq +1.5^\circ$ ;  $-80^\circ \leq l \leq -60^\circ$ , and  $-2.0^\circ \leq b \leq +1.0^\circ$ ). More than 10000 compact submillimeter sources (dense clumps) were identified (Contreras et al. 2013; Csengeri et al. 2014).

In addition, the dense regions of molecular gas can be detected by using molecular lines tracing high density environments, e.g.,  $\text{HCO}^+$ ,  $\text{NH}_3$  (Purcell et al. 2012; Shirley et al. 2013). The  $\text{H}_2\text{O}$  Southern Galactic Plane Survey (HOPS) maps the inner Galactic plane ( $-70^\circ > l > 30^\circ$ ,  $|b| < 0.5^\circ$ ) using the Mopra 22m telescope at  $12\text{ mm}$  wavelengths ( $19.5\text{--}27.5\text{ GHz}$ , Walsh et al. 2011), and detect 669 dense clouds by using  $\text{NH}_3(1,1)$  transition (Purcell et al. 2012).

The number density of the dense clumps from the ATLASGAL and HOPS is plotted against the Galactic longitude in the panel <5> of Fig. 2. The arm tangencies for the northern part of the Near 3 kpc Arm ( $l \sim 24^\circ$ ), the Scutum Arm ( $l \sim 32^\circ$ ), and the Sagittarius Arm ( $l \sim 50^\circ$ ) can be easily identified from the longitude plot without ambiguity. Similar to the number density plots for HII regions and methanol masers, the bump features in the fourth Galactic quadrant are complex, and need to be compared to arm tangency directions obtained from the RRL/CO/HI plots. The identified bump peaks indicate the concentration of dense clumps around spiral arms, which can be taken as the “observed” arm tangencies from high density gas clumps.

## 2.4 Atomic gas: HI

Atomic gas in our Galaxy has been extensively observed by HI 21cm line with low resolution in early days and more recently at high resolution (McClure-Griffiths et al. 2005; Stil et al. 2006).

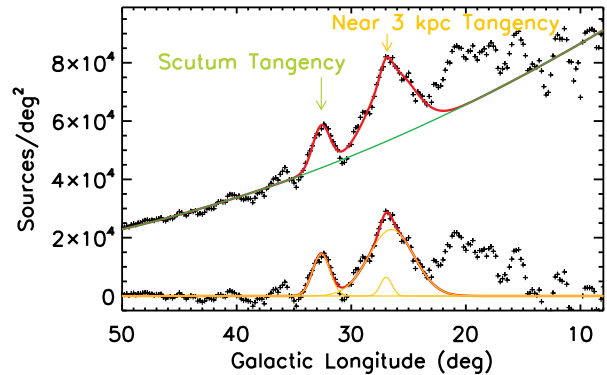


**Figure 3.** An example of fitting the longitude plot of old stars for the tangency of the Scutum Arm and the northern tangency of the Near 3 kpc Arm. The surface density of stars are deduced from the GLIMPSE  $4.5\text{ }\mu\text{m}$  data. The “baseline” (green) is subtracted first (black crosses in the bottom), and then three Gaussians (yellow) are fitted to the data.

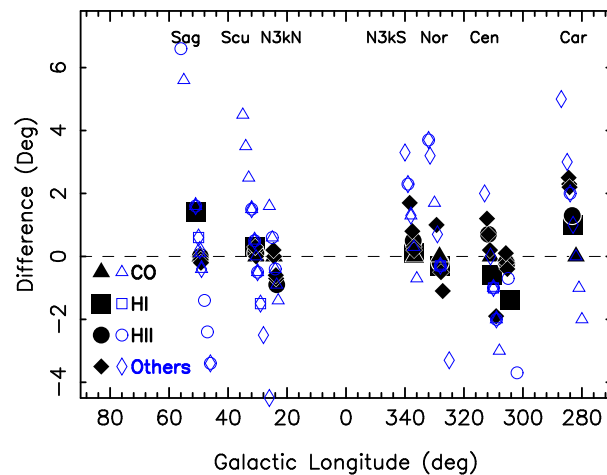


**Figure 4.** The longitude values of arm tangencies for different spiral components comparing with those determined by  $^{12}\text{CO}$  in this paper. Filled symbols indicate the assessments in this paper, and the open symbols stand for the values in literature (see Englmaier & Gerhard 1999; Hou & Han 2014; Vallée 2014a).

The Leiden/Argentine/Bonn (LAB) survey covering the entire sky is the most sensitive HI survey to date (Kalberla et al. 2005), which merges the Leiden/Dwingeloo survey of the northern sky (Hartmann & Burton 1997) and the Instituto Argentino de Radioastronomía Survey of the southern sky (Arnal et al. 2000; Bajaja et al. 2005). The angular resolution is  $\sim 36'$ . The LSR velocity coverage is from  $-450\text{ km s}^{-1}$  to  $+400\text{ km s}^{-1}$ . The rms noise of the data is  $70\text{ mK} - 90\text{ mK}$ .

Similar to the RRL plot and the CO plot, the integrated HI intensity over  $|b| < 2^\circ$  and a velocity range of  $\Delta V = [V_t - 15\text{ km s}^{-1}, V_t + 15\text{ km s}^{-1}]$  around the terminal velocity is plotted in the panel <6> of Fig. 2. The atomic gas is not obviously concentrated to spiral arms as molecular gas (also see Nakanishi & Sofue 2003, 2006), so that the bump features in the HI plot are not as prominent as those in the RRL and CO plots. The known arm tangencies, however, can be recognized except for the northern tangency of the Near 3 kpc Arm ( $l \sim 24^\circ$ ). The bump peaks in the HI plot indicate the density maximums of atomic gas in spiral arms.

**Table 1.** The Galactic longitudes of “observed” spiral arm tangencies of the Milky Way recognized from the survey data of old stars, RRLs, HII regions, methanol masers, CO, dense clumps, and HI. The measured bump widths in FWHM are given in brackets. The median values of arm tangencies for stars (GLIMPSE/2MASS) and gas (RRLs, HII regions, masers, CO, dense clumps, and HI) are given in the bottom. Values with “\*” have the significance of identified bump less than  $3\sigma$ .

Survey Data	Near 3 kpc North (°)	Scutum (°)	Sagittarius (°)	Carina (°)	Centaurus (°)	Norma (°)	Near 3 kpc South (°)
GLIMPSE 3.6 $\mu\text{m}$	26.9 [3.2]	32.6 [1.7]	—	—	307.5 [4.0]	—	338.3 [4.8]
GLIMPSE 4.5 $\mu\text{m}$	26.9 [3.8]	32.6 [1.8]	—	—	307.6 [5.1]	—	338.3 [5.1]
GLIMPSE 5.8 $\mu\text{m}$	27.1 [3.3]	32.7 [1.6]	—	—	307.4 [4.3]	—	337.7 [2.4]
GLIMPSE 8.0 $\mu\text{m}$	27.4 [1.5]	32.8 [1.2]	—	—	307.3 [1.9]	—	337.8 [0.9]
2MASS $K_s$ (2.16 $\mu\text{m}$ )	27.0 [2.3]	32.6 [1.5]	55.0* [2.7]	—	307.5 [2.9]	—	338.3 [3.6]
2MASS $H$ (1.65 $\mu\text{m}$ )	27.0 [2.1]	32.6 [1.4]	55.0* [2.6]	—	307.5 [2.5]	—	338.3 [2.9]
2MASS $J$ (1.25 $\mu\text{m}$ )	27.1 [2.1]	32.5 [1.4]	55.0* [2.3]	—	307.1 [2.1]	—	338.3 [1.7]
1.4-GHz RRLs	24.6 [0.7]	30.8 [0.7]	49.2 [0.8]	284.3 [0.6]	305.4 [0.7], 311.2 [0.9]	329.3 [1.9]	336.9* [0.6]
WISE HII regions	23.5* [2.1]	30.6 [1.5]	49.4 [1.0]	283.3* [2.1]	305.5 [0.8], 311.7 [1.8]	328.1 [2.2]	337.2 [1.0]
6.7-GHz methanol masers	24.6* [0.7]	30.8 [0.9]	49.3 [0.8]	284.5* [0.5]	305.5 [0.9], 312.2 [1.1]	329.3 [2.9]	337.0 [2.8]
$^{12}\text{CO}$ (DHT2001)	24.4 [0.3]	30.5 [2.0]	49.4 [0.5]	282.0 [2.7]	305.7 [5.2], 311.0 [4.6]	328.3 [2.2]	336.7* [0.8]
$^{13}\text{CO}$ (GRS)	24.4 [0.4]	30.5 [1.6]	49.4 [0.5]	—	—	—	—
ATLASGAL dust sources	23.8 [1.7]	30.7 [0.9]	49.2 [0.7]	284.2* [0.5]	305.3 [0.8], 311.7* [1.0]	327.2 [2.5]	337.5 [2.6]
HOPS $\text{NH}_3$ sources	23.7 [2.3]	—	—	—	305.8 [1.5], 309.1 [0.6]	327.8 [2.1]	338.4 [2.5]
HI (LAB)	—	30.8 [2.3]	50.8 [5.8]	283.0 [9.3]	304.3 [14.1], 310.4 [6.4]	328.0 [4.5]	336.8 [5.7]
Median for old stars	27.0	32.6	55.0	—	307.5	—	338.3
Median for gas	24.4	30.7	49.4	283.8	305.5, 311.2	328.1	337.0

### 3 ARM TANGENCIES FOR DIFFERENT COMPONENTS

#### 3.1 Measuring arm tangencies from the longitude plots

As discussed above, the peaks of the bumps in the longitude plots correspond to the arm tangencies (see Fig. 2). To measure the peak position, we first fit the “baseline” with a second-order polynomial function outside the tangency range which should represent the general contribution from the Galaxy disk. The baseline is then subtracted from data to show bumps more clearly. After that a single Gaussian or multi-gaussians are fitted to a bump, as shown in Fig. 3. The peak position of the fitted Gaussian(s) is adopted as the longitude direction of “observed” arm tangency, and the bump width is derived as well to be the full width at half maximum (FWHM), as listed in Table 1. We noticed that for each arm the tangency longitudes derived from the gaseous components (RRLs, star formation sites, CO, HI, dense clumps) have similar values, with a much smaller difference than various values in literature (see Fig. 4). We verified that results change less than  $1^\circ$  if other fitting functions are used, e.g., a single Gaussian plus a first-order polynomial function.

Note also that a flat rotation curve with the IAU standard circular orbital speed at the Sun of  $\Theta_0 = 220 \text{ km s}^{-1}$  is adopted to calculate the terminal velocity  $V_t$ , and then the velocity range of  $\Delta V = V_t \pm 15 \text{ km s}^{-1}$  for the integrated line intensity is used to derive the longitude plots for RRLs, CO and HI in Fig. 2. We tested and found that if the other rotation curves, e.g. the one given by Brand & Blitz (1993), Clemens (1985), and Fich et al. (1989), or different  $\Theta_0$  (238 – 240  $\text{km s}^{-1}$ , Schönrich 2012; Reid et al. 2014), or even the different velocity ranges such as  $\pm 5 - \pm 25 \text{ km s}^{-1}$ , are used, the measured arm tangencies change less than  $\sim 0.5^\circ$  and the measured bump widths change less than  $\sim 1^\circ$ . So does the magnitude range for the old stars.

#### 3.2 “Observed” tangencies and the true density peaks

To explain the detailed features in the plots of Fig. 2, an illuminating model should include disk, bulge, Galactic bar(s), spiral arms, and also interstellar extinction and luminosity function (e.g., Ortiz & Lepine 1993; Drimmel 2000; Robitaille et al. 2012; Polido et al. 2013). Here, we try to understand the interplay between the observed bumps for arm tangencies and the true density peaks in spiral arms. For this purpose, we make a simplified model as shown in Fig. 5, which consists of two density components (see Drimmel & Spergel 2001):

$$\rho = \rho_{\text{disk}} + \rho_{\text{arm}} = A_{\text{disk}} \exp(-r/h_r) + A_{\text{arm}} \sum_i \exp(-d_i/w_i)^2. \quad (1)$$

Here,  $\rho_{\text{disk}}$  is an axisymmetric exponential disk,  $\rho_{\text{arm}}$  comes from spiral arms,  $r$  is the Galactocentric distance,  $h_r$  is the scale length,  $d_i$  is the distance to the nearest spiral arm,  $w_i(r) \propto r$  indicates the half-width of the  $i$ th arm, and  $A_{\text{disk}}$  and  $A_{\text{arm}}$  are the density normalization for the disk and spiral arms, respectively. The density profile acrosses an arm is taken as Gaussian. The polynomial-logarithmic model derived by fitting to the distribution of HII regions by Hou & Han (2014, see the *left* panel in their Fig. 11) is adopted for the spiral arms, which have the known density peaks at arm tangencies of spiral arms. We put  $10^6$  particles randomly to match the density model in Fig. 5.

According to Binney & Merrifield (1998), the number of stars of type  $s$  with apparent magnitude between  $m_1$  and  $m_2$  in a solid angle  $d\Omega$  in the  $(l, b)$  direction is:

$$N_s(m_1, m_2, l, b) d\Omega = \int_{m_1}^{m_2} dm \int_0^\infty \rho_s(R, l, b, M) \Phi_s(M) R^2 dR d\Omega, \quad (2)$$

here,  $R$  is the heliocentric distance,  $M$  is the absolute magnitude,  $\rho_s$  is the stellar density near the Galactic plane, and  $\Phi_s$  is the luminosity function of stars of type  $s$ . Because a good fraction of GLIMPSE detected stars appear to be red-clump giants (Churchwell et al.



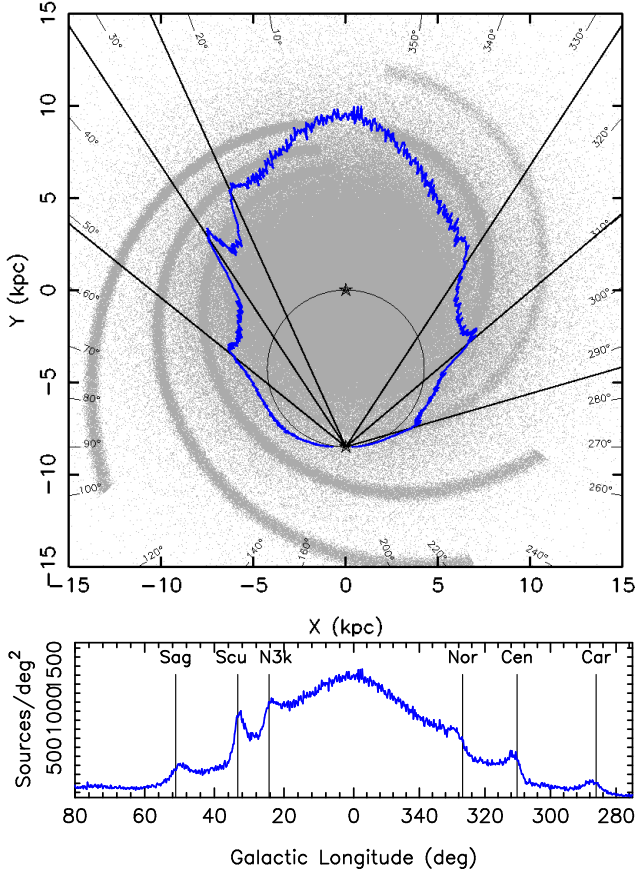


**Figure 5.** The density model (the upper panel) and the surface density of old stars as a function of the Galactic longitude (the lower panel). The “observed” arm tangencies can be identified by the bump peaks. The “true” density peaks near spiral arm tangencies in the model are indicated by solid lines, which are displaced from the “observed” bump peaks.

2009), it would be reasonable to assume that the bump features shown in the infrared star counts are dominated by red-clump giants. We assume that the stellar density is proportional to the density model given in Eq. (1). Considering that the GLIMPSE mid-infrared survey allowed for the nearly-extinction free detection of stars in the inner Galactic plane (Benjamin 2008), and also for simplicity, we neglect the extinction effect. The luminosity function of red-clump giants given by Alves (2000, see their Fig.3) is normalized and adopted, and the apparent magnitude range between  $m_1 = 6.5$  and  $m_2 = 12.5$  is adopted in the calculations. Then the longitude plot for the surface density of stars can be derived as shown in the lower panel of Fig. 5, with clear bump features for arm tangencies.

We find that the directions for “observed” arm tangencies deviate from the longitudes of the “true” density maximums of spiral arms near the tangencies by shifting to the inner side of about  $1^\circ$  in general (see Fig. 6), depending on the input arm width in the model. Near the Norma tangency, the shift could be as large as  $2.5^\circ$  if the arm has a width (FWHM) of  $0.4 \text{ kpc} - 0.5 \text{ kpc}$ .

Similar simulations for gas distributions can be obtained to get the modeled longitude plots of integrated intensities. Take the CO data as an example. The integrated emission  $W(l, b)_{\text{CO}} d\Omega = \int T_R(l, b, v) dv d\Omega$  is commonly assumed to be proportional to the column density of molecular hydrogen  $N(H_2)$ , e.g.,  $N(H_2) = XW(\text{CO})$ . Here  $X$  is the conversion factor,  $T_R(l, b, v)$  is the CO

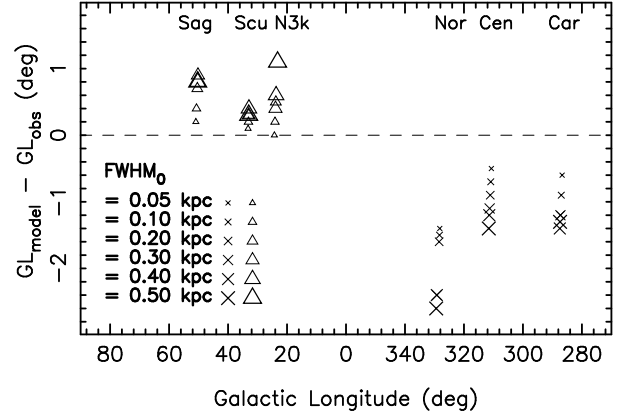


**Figure 6.** The “observed” longitude values for arm tangencies ( $GL_{\text{obs}}$ ) deduced from various simulated models with a different input arm width ( $\text{FWHM}_0$ ). The “observed” tangency directions are shifted to the interior to the “true” arm density peaks of the model ( $GL_{\text{model}}$ ).

line temperature (e.g., Grabelsky et al. 1987). Hence,  $dN(H_2) = \rho(R, l, b) dR = XT_R(l, b, v) dv$ , where  $\rho(R, l, b)$  is the gas density,  $R$  is the heliocentric distance. Then the integrated intensity of CO:

$$\int T_R dv d\Omega \propto \int \rho(R, l, b) dR d\Omega \quad (3)$$

can be obtained from the density model (see Fig. 5). We get the same conclusion for gas arms as that for the stellar arms.

More sophisticated model could be constructed to explain the real data. For example, the infrared stars in the GLIMPSE and 2MASS surveys consist of a mixture of different types of stars with different luminosity functions, and distant stars should suffer from extinction effect. The optical depth and beam dilution effects should be considered in the gas density model. However, the very simplified models discussed above seem to be good enough to illustrate the interplay between the observed bumps and the true density peaks near the spiral arm tangencies.

### 3.3 Displacements of spiral arms outlined by different tracers

The measured directions for tangencies are not exactly the real directions of density peaks of spiral arms near the tangencies, with a slight shift to the interior to the arm. However such a shift happens to all kinds of spiral tracers, various gas arms or stellar arms. Therefore, the *relative* longitude positions of arm tangencies shown by different components can be used to check the spatial coincidence of different spiral arm components.

For the tangencies of the Scutum-Centaurus Arm and the northern and southern parts of the Near 3 kpc Arm, the consistent longitude is found for the stellar arm tangency from the infrared data of GLIMPSE and 2MASS (see Fig. 7 and also Table 1) although the extinction is significantly less at GLIMPSE  $4.5 \mu\text{m}$  band than the 2MASS  $J$ ,  $H$ , and  $K_s$  bands (Fig. 2).

Arm tangencies shown by RRLs, HII regions, methanol masers, CO, dense clumps, and HI data have more or less similar longitudes (see Fig. 7) with a small difference of  $\leq 1.1^\circ$  ( $\sim 150 \text{ pc}$ ) for the northern tangency of the Near 3 kpc Arm,  $\leq 0.3^\circ$  ( $\sim 40 \text{ pc}$ ) for the Scutum tangency,  $\leq 1.6^\circ$  ( $\sim 150 \text{ pc}$ ) for the Sagittarius tangency,  $\leq 2.5^\circ$  ( $\sim 90 \text{ pc}$ ) for the Carina tangency,  $\leq 2.1^\circ$  ( $\sim 260 \text{ pc}$ ) for the Norma tangency, and  $\leq 1.7^\circ$  ( $\sim 230 \text{ pc}$ ) for the Southern Near 3 kpc tangency, which are comparable to the typical uncertainty of the measured arm tangencies ( $\sim 1^\circ$ ), and smaller

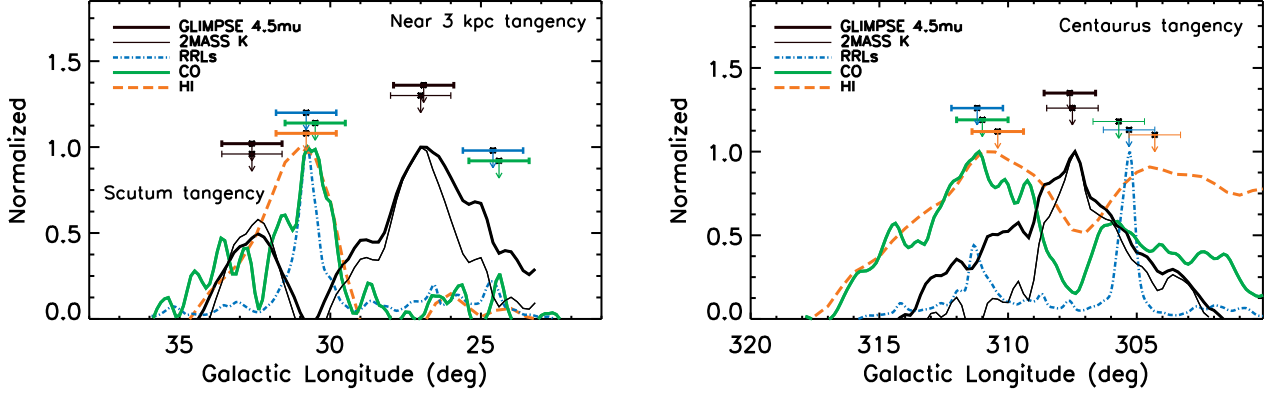


**Figure 7.** The longitude plots after “baseline” subtracted (see Fig. 2 and Fig. 3) for the tangency of the Scutum Arm and the northern tangency of the Near 3 kpc Arm (*left panel*) and the Centaurus Arm (*right panel*), normalized by the maximum values in each plot. The tangencies are indicated by arrows together with typical uncertainties less than  $1^\circ$ .

than the widths of spiral arms in our Galaxy ( $\sim 200$  pc –  $400$  pc, Reid et al. 2014). The Centaurus tangency region ( $l \sim 302^\circ - 313^\circ$ ) seems complex, which is known for several anomalies (Benjamin 2008). It has two distinct gas components (see Fig. 2 and Fig. 7), one is near  $l \sim 311^\circ$  and another is near  $l \sim 306^\circ$ . The longitude difference for each component near the Centaurus tangency shown by RRLs, CO, and HI is small,  $\leq 1.4^\circ$  ( $\sim 120$  pc). Therefore, there is almost no obvious and ordered shift for spiral arms traced by different gas tracers, i.e., RRLs, HII regions, methanol masers, CO, dense gas regions, and HI.

However, remarkable difference is found between the arm tangencies traced by old stars and gas (see Fig. 7), which is about  $2.3^\circ - 3.9^\circ$  ( $\sim 310$  pc –  $520$  pc) for the northern part of the Near 3 kpc Arm,  $1.7^\circ - 2.3^\circ$  in the Galactic longitude ( $\sim 210$  pc –  $290$  pc) for the Scutum Arm, and about  $1.3^\circ - 5.1^\circ$  ( $\sim 120$  pc –  $480$  pc) for the Centaurus Arm, which are comparable to the widths of spiral arms. In the tangency regions of the northern part of the Near 3 kpc Arm and the Scutum Arm, the stellar arms are exterior to the gas arms. As for the Centaurus tangency, the offset direction of stellar arm relative to gas arm is complex as it has two distinct gaseous components. The relative strength of these two components shown by different gas tracers (RRLs, CO, and HI) are not consistent (Fig. 7). The CO/HI integrated intensity for the component near  $l \sim 311^\circ$  is stronger than that for the component near  $l \sim 305^\circ$  (Fig. 7). By comparing the bump profiles derived from the 2MASS  $K_s$  band data and the GLIMPSE  $4.5\mu\text{m}$  data (see the right panel in Fig. 7), we found that the number increase of infrared stars detected by GLIMPSE in the longitude range of  $l \sim 309^\circ - 314^\circ$  is much more prominent than that in the longitude range of  $l \sim 302^\circ - 307^\circ$ . Hence, the extinction caused by interstellar dust is much more serious in the  $l \sim 309^\circ - 314^\circ$  directions, indicating a larger dust and gas content. In addition, the literature mean values of the Centaurus tangency (see the summary given by Englmaier & Gerhard 1999; Vallée 2014a) are commonly adopted as  $\sim 309^\circ$ , closer to the gas component near  $l \sim 311^\circ$ . These features indicate that the bump component near  $l \sim 311^\circ$  have a stronger gas concentration and larger gas content, and the stellar Centaurus Arm is exterior to this component. The shift of stellar arms exterior to CO gas arms increases with the Galactocentric radius. Such offsets has also been observed in some nearby galaxies (e.g., M81, Kendall et al. 2008).

Therefore, to identify the arm tangency features from the star count plots, the possible offset between the stellar arms and gas

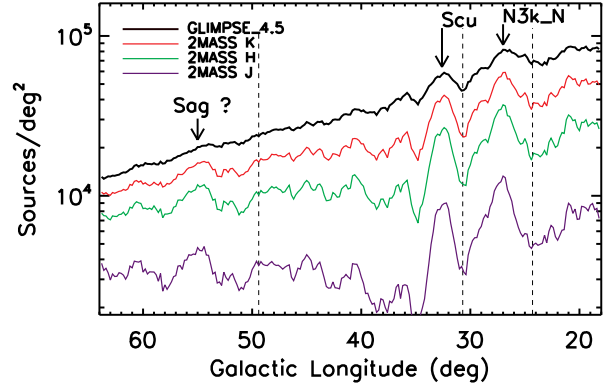


**Figure 8.** Surface density of infrared stars as a function of the Galactic longitude, deduced from the survey data of GLIMPSE  $4.5\mu\text{m}$ , 2MASS  $K_s$ ,  $H$ , and  $J$  bands. The arm tangencies in longitudes for the northern part of the Near 3 kpc Arm (N3k\_N), the Scutum Arm (Scu), and the possible Sagittarius Arm (Sag) are indicated by arrows for the stellar components, and by dashed lines for the gaseous components.

arms should be considered. We re-check the star count plots and found that the stellar data from 2MASS  $J$ ,  $H$ , and  $K_s$  bands show a broad but small amplitude bump in the longitude plot near Galactic longitude  $\sim 55^\circ$  (see Fig. 8). This bump, which has not been identified (e.g., see Drimmel 2000; Churchwell et al. 2009), may be related to the tangency of the Sagittarius Arm but shifted about  $4.2^\circ - 5.8^\circ$  ( $\sim 380$  pc –  $530$  pc) exterior to the gas arm. This direction offset is consistent with the offsets for the Scutum Arm, the northern part of the Near 3 kpc Arm, and the Centaurus Arm, and the offset value ( $\sim 4.2^\circ - 5.8^\circ$ ) is larger but comparable to that for the Centaurus Arm ( $\sim 1.3^\circ - 5.1^\circ$ ).

For the southern tangency of the Near 3 kpc Arm, the difference between the arm tangency traced by stars and gas is not significant, and around the tangency directions of the Carina Arm and the Norma Arm, no obvious bumps can be found in the stellar data, so that for these arms the possible displacements can not be properly assessed.



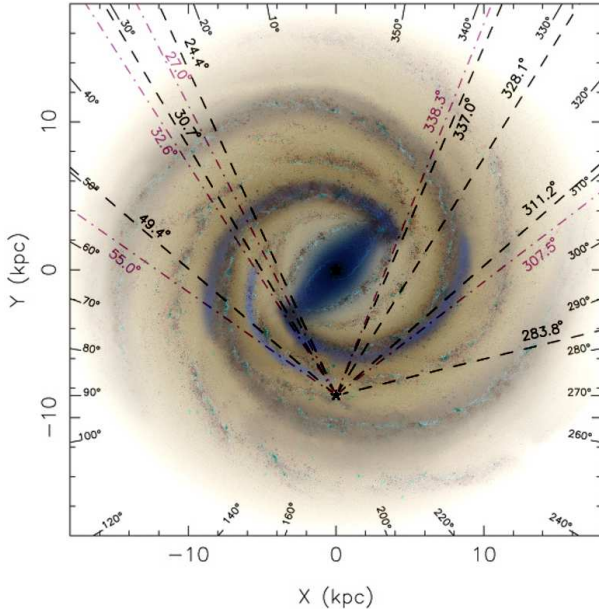


**Figure 9.** A face-on image of the Milky Way modified from the artist’s map (NASA/JPL-Caltech/R. Hurt) to match the observational properties summarized in this paper. The gaseous components in the Galactic plane are dominated by four arm segments (see Hou & Han 2014). The stellar component is dominated by a two-arm spiral pattern but with a third weaker stellar arm of the Sagittarius. The newly derived arm tangencies in this paper are indicated by dashed lines for the gas arms, and dot-dashed lines for the stellar arms.

#### 4 DISCUSSIONS AND CONCLUSIONS

We reassess the Galactic longitude directions of spiral arm tangencies in the Milky Way by using survey data for infrared stars and RRLs, HII regions, 6.7 GHz methanol masers, CO, high density regions in gas, and HI with a consistent definition for the tangencies. As verified by a simple model, the directions of arm tangencies are very close to the real density peaks of spiral arms near tangencies, but have a shift of about  $1^\circ$  to the interior to the arm and the shift happens to all kinds of spiral tracers.

Spiral arm tangency directions derived by different gas tracers, i.e., RRLs, HII regions, methanol masers, CO, dense gas, and HI, are almost at the same longitudes for the Scutum-Centaurus Arm, the Sagittarius-Carina Arm, the Norma Arm, and the Near 3 kpc Arm. Therefore, we conclude that there is no obvious shift between the gas arms, in spite of the gas phases, ionized or neutral or molecular.

We derived the tangency directions for the stellar arms, the Scutum-Centaurus Arm, the Near 3 kpc Arm, and the Sagittarius Arm, and obtain consistent values of arm tangencies by using stellar data of GLIMPSE and 2MASS. However, we find remarkable difference between the tangency directions of the stellar arms and the gas arms for the Scutum-Centaurus Arm, the northern part of the Near 3 kpc Arm and maybe the Sagittarius Arm, with a shift about  $1.3^\circ$ – $5.8^\circ$  ( $\sim 120$  pc – 530 pc) in the Galactic longitude for different arms, nearly about the widths of spiral arms in our Galaxy ( $\sim 200$  pc – 400 pc). The obvious offset between the stellar component near  $l \sim 27^\circ$  and gas components near  $l \sim 24^\circ$  for the Near 3 kpc Arm deserves further studies since it could be related to a barred potential (e.g.,  $l \sim 27^\circ$ , López-Corredoira et al. 2001; Benjamin et al. 2005). The double peaks for gas components near the Centaurus tangency are intriguing and deserve for further inves-

tigations. The stellar overdensity near  $l \sim 55^\circ$  shown by using the 2MASS  $J$ ,  $H$  and  $K_s$  band data maybe related to the tangency of the stellar Sagittarius Arm, though the feature is not obvious in the GLIMPSE data. The stellar Sagittarius Arm may be much weaker than the stellar Scutum-Centaurus Arm, and was smeared out in the GLIMPSE data. It is also possible that the stellar overdensity shown in 2MASS data is caused by some nearby stellar structures, and not related to the Sagittarius tangency. This intriguing feature deserves further attention as it is important to better understand the stellar density distribution in the Galactic disk.

Based on observational properties of spiral structure we construct a face-on image for the Milky Way as shown in Fig. 9, which shows that the gaseous components are dominated by four arm segments in the inner Galaxy regions (e.g., Georgelin & Georgelin 1976; Russeil 2003; Hou et al. 2009; Hou & Han 2014), and may extend to the far outer Galaxy (e.g., Hou & Han 2014; Sun et al. 2015). The Local Arm is probably an branch of the Perseus Arm (e.g., Xu et al. 2013; Hou & Han 2014; Burns et al. 2014). The distribution of old stars in the Galactic plane is dominated by a two-arm spiral pattern (two major spiral arms: the Scutum-Centaurus Arm and the Perseus Arm, e.g., Drimmel 2000; Drimmel & Spergel 2001; Benjamin et al. 2005; Churchwell et al. 2009; Francis & Anderson 2012). The Sagittarius Arm may be the third but a weaker stellar arm. The tangency directions for the density maximums of gas arm and stellar arm for the Scutum-Centaurus Arm has a longitude difference as large as  $1.6^\circ$ – $4.7^\circ$  ( $\sim 150$  pc – 420 pc). In the inner Galaxy, the stellar arms are shifted outwards with respect to the gaseous arms traced by RRLs, CO and HI, not only for the Scutum-Centaurus Arm, the northern part of the Near 3 kpc Arm, but maybe also for the Sagittarius Arm.

Among three proposed mechanisms to produce spiral arms in galaxies, only the quasi-stationary density wave theory predicts a spatial displacement between the density peaks traced by stars and gas in spiral arms, by assuming a constant pattern speed (e.g., Roberts 1969; Dobbs & Baba 2014, and see Fig. 1). Our data analyses show the shift between the directions for the density maximums of stars and the intensity peaks for gas emission in the Scutum-Centaurus Arm near the tangencies, which is evidence for the quasi-stationary density wave in the Milky Way. Considering the symmetry of the Galaxy spiral structure proposed in literature (e.g., Dame 2013), such an offset between gas and old stars is also expected in the Perseus Arm (see Fig. 9), and recently discussed by Monguió et al. (2015) using the stellar overdensity and the interstellar visual absorption in the anticenter direction. The accurate measurements of the parallax/proper motion for stars by Gaia (e.g., Robin et al. 2012; Kawata et al. 2015), and for high-mass star forming regions by the Bar and Spiral Structure Legacy (BeSSel) Survey<sup>4</sup> and the Japanese VLBI Exploration of Radio Astrometry (VERA)<sup>5</sup> will provide critical tests in the near future. In addition, no *general* spatial ordering can be reliably deduced for the multiphase gas arms. Considering the multiphase properties of interstellar medium and the stellar feedback (e.g., Wada 2008), the response of gas to the Galaxy potential probably highly complex, making it difficult to verify the possible spatial ordering for multiphase gas arms in observations at present.

<sup>4</sup> <http://bessel.vlbi-astrometry.org>

<sup>5</sup> <http://veraserver.mtk.nao.ac.jp>

## ACKNOWLEDGEMENTS

We appreciate the anonymous referee for the instructive comments which help us to improve the paper. The authors are supported by the Strategic Priority Research Program “The Emergence of Cosmological Structures” of the Chinese Academy of Sciences, Grant No. XDB09010200, and the National Natural Science Foundation (NNSF) of China No. 11473034. L.G.H. is also supported by the Young Researcher Grant of National Astronomical Observatories, Chinese Academy of Sciences.

## REFERENCES

- Aguirre, J. E., Ginsburg, A. G., Dunham, M. K., et al. 2011, *ApJS*, 192, 4
- Alvarez, H., May, J., & Bronfman, L. 1990, *ApJ*, 348, 495
- Alves, D. R. 2000, *ApJ*, 539, 732
- Alves, M. I. R., Calabretta, M., Davies, R. D., et al. 2015, *MNRAS*, 450, 2025
- Alves, M. I. R., Davies, R. D., Dickinson, C., et al. 2010, *MNRAS*, 405, 1654
- Anderson, L. D., Bania, T. M., Balser, D. S., et al. 2014, *ApJS*, 212, 1
- Andre, P., Ward-Thompson, D., & Barsony, M. 2000, *Protostars and Planets IV*, 59
- Arnal, E. M., Bajaja, E., Larrarte, J. J., Morras, R., & Pöppel, W. G. L. 2000, *A&AS*, 142, 35
- Baba, J., Morokuma-Matsui, K., & Egusa, F. 2015, *arXiv:1505.02881*
- Bajaja, E., Arnal, E. M., Larrarte, J. J., et al. 2005, *A&A*, 440, 767
- Bania, T. M. 1980, *ApJ*, 242, 95
- Battisti, A. J., & Heyer, M. H. 2014, *ApJ*, 780, 173
- Benjamin, R. A. 2009, in *IAU Symposium*, Vol. 254, IAU Symposium, ed. J. Andersen, Nordströara, B. m, & J. Bland-Hawthorn, 319–322
- Benjamin, R. A. 2008, *Massive Star Formation: Observations Confront Theory*, 387, 375
- Benjamin, R. A., Churchwell, E., Babler, B. L., et al. 2005, *ApJL*, 630, L149
- Benjamin, R. A., Churchwell, E., Babler, B. L., et al. 2003, *PASP*, 115, 953
- Beuermann, K., Kanbach, G., & Berkhuijsen, E. M. 1985, *A&A*, 153, 17
- Beuther, H., Tackenberg, J., Linz, H., et al. 2012, *ApJ*, 747, 43
- Bihl, S., Beuther, H., Ott, J., et al. 2015, *arXiv:1505.05176*
- Binney, J. & Merrifield, M. 1998, *Galactic Astronomy*
- Binney, J. & Tremaine, S. 2008, *Galactic Dynamics: Second Edition* (Princeton University Press)
- Bissantz, N., Englmaier, P., & Gerhard, O. 2003, *MNRAS*, 340, 949
- Bloemen, J. B. G. M., Deul, E. R., & Thaddeus, P. 1990, *A&A*, 233, 437
- Brand, J., & Blitz, L. 1993, *A&A*, 275, 67
- Breen, S. L., Fuller, G. A., Caswell, J. L., et al. 2015, *MNRAS*, 450, 4109
- Bronfman, L., Alvarez, H., Cohen, R. S., & Thaddeus, P. 1989, *ApJS*, 71, 481
- Bronfman, L., Casassus, S., May, J., & Nyman, L.-Å. 2000a, *A&A*, 358, 521
- Bronfman, L., Cohen, R. S., Alvarez, H., May, J., & Thaddeus, P. 1988, *ApJ*, 324, 248
- Bronfman, L., May, J., & Luna, A. 2000b, in *Astronomical Society of the Pacific Conference Series*, Vol. 217, *Imaging at Radio through Submillimeter Wavelengths*, ed. J. G. Mangum & S. J. E. Radford, 66
- Burns, R. A., Nagayama, T., Handa, T., et al. 2014, *ApJ*, 797, 39
- Burton, W. B. & Shane, W. W. 1970, in *IAU Symposium*, Vol. 38, *The Spiral Structure of our Galaxy*, ed. W. Becker & G. I. Kontopoulos, 397
- Burton, W. B. 1971, *A&A*, 10, 76
- Burton, W. B. 1973, *PASP*, 85, 679
- Cabrera-Lavers, A., Hammersley, P. L., González-Fernández, C., et al. 2007, *A&A*, 465, 825
- Carraro, G. 2015, *arXiv:1502.03151*
- Caswell, J. L., Fuller, G. A., Green, J. A., et al. 2010, *MNRAS*, 404, 1029
- Caswell, J. L., Fuller, G. A., Green, J. A., et al. 2011, *MNRAS*, 417, 1964
- Churchwell, E., Babler, B. L., Meade, M. R., et al. 2009, *PASP*, 121, 213
- Clemens, D. P. 1985, *ApJ*, 295, 422
- Cohen, R. J. & Davies, R. D. 1976, *MNRAS*, 175, 1
- Contreras, Y., Schuller, F., Urquhart, J. S., et al. 2013, *A&A*, 549, A45
- Cordes, J. M. & Lazio, T. J. W. 2002, *arXiv: astro-ph/0207156*
- Csengeri, T., Urquhart, J. S., Schuller, F., et al. 2014, *A&A*, 565, A75
- Cyganowski, C. J., Brogan, C. L., Hunter, T. R., & Churchwell, E. 2009, *ApJ*, 702, 1615
- Dame, T. M., Elmegreen, B. G., Cohen, R. S., & Thaddeus, P. 1986, *ApJ*, 305, 892
- Dame, T. M., Hartmann, D., & Thaddeus, P. 2001, *ApJ*, 547, 792
- Dame, T. M. & Thaddeus, P. 2008, *ApJL*, 683, L143
- Dame, T. M. & Thaddeus, P. 2011, *ApJL*, 734, L24
- Dame, T. M. 2013, in *American Astronomical Society Meeting Abstracts*, Vol. 222, *American Astronomical Society Meeting Abstracts*, 400.01
- Dobbs, C. & Baba, J. 2014, *PASA*, 31, 35
- Downes, D., Wilson, T. L., Bieging, J., & Wink, J. 1980, *A&AS*, 40, 379
- Drimmel, R. 2000, *A&A*, 358, L13
- Drimmel, R. & Spergel, D. N. 2001, *ApJ*, 556, 181
- Egusa, F., Kohno, K., Sofue, Y., Nakanishi, H., & Komugi, S. 2009, *ApJ*, 697, 1870
- Ellingsen, S. P. 2007, *MNRAS*, 377, 571
- Elmegreen, B. G. 1990, *Annals of the New York Academy of Sciences*, 596, 40
- Englmaier, P. & Gerhard, O. 1999, *MNRAS*, 304, 512
- Ferrière, K. M. 2001, *Reviews of Modern Physics*, 73, 1031
- Fich, M., Blitz, L., & Stark, A. A. 1989, *ApJ*, 342, 272
- Fontani, F., Cesaroni, R., & Furuya, R. S. 2010, *A&A*, 517, A56
- Foyle, K., Rix, H.-W., Dobbs, C. L., Leroy, A. K., & Walter, F. 2011, *ApJ*, 735, 101
- Foster, T., & Cooper, B. 2010, *The Dynamic Interstellar Medium: A Celebration of the Canadian Galactic Plane Survey*, 438, 16
- Francis, C. & Anderson, E. 2012, *MNRAS*, 422, 1283
- Fux, R. 1999, *A&A*, 345, 787
- Georgelin, Y. M. & Georgelin, Y. P. 1976, *A&A*, 49, 57
- Ginsburg, A., Glenn, J., Rosolowsky, E., et al. 2013, *ApJS*, 208, 14
- Gordon, M. A., & Soroichenko, R. L. 2009, *Astrophysics and Space Science Library*, 282,
- Grabelsky, D. A., Cohen, R. S., Bronfman, L., Thaddeus, P., & May, J. 1987, *ApJ*, 315, 122
- Green, J. A., Caswell, J. L., Fuller, G. A., et al. 2009, *MNRAS*, 392, 783
- Green, J. A., Caswell, J. L., Fuller, G. A., et al. 2010, *MNRAS*, 409, 913
- Green, J. A., Caswell, J. L., Fuller, G. A., et al. 2012, *MNRAS*, 420, 3108
- Green, J. A., Caswell, J. L., McClure-Griffiths, N. M., et al. 2011, *ApJ*, 733, 27
- Hartmann, D. & Burton, W. B. 1997, *Atlas of Galactic Neutral Hydrogen*
- Hayakawa, S., Matsumoto, T., Murakami, H., et al. 1981, *A&A*, 100, 116
- Hou, L. G. & Han, J. L. 2014, *A&A*, 569, A125
- Hou, L. G., Han, J. L., & Shi, W. B. 2009, *A&A*, 499, 473
- Hubble, E. P. 1926, *ApJ*, 63, 236
- Jackson, J. M., Rathborne, J. M., Shah, R. Y., et al. 2006, *ApJS*, 163, 145
- Kendall, S., Kennicutt, R. C., Clarke, C., & Thornley, M. D. 2008, *MNRAS*, 387, 1007
- Kalberla, P. M. W., Burton, W. B., Hartmann, D., et al. 2005, *A&A*, 440, 775
- Kawata, D., Hunt, J. A. S., Grand, R. J. J., et al. 2015, *arXiv:1502.03570*
- Lequeux, J. 2005, *The interstellar medium, Translation from the French language edition of: Le Milieu Interstellaire by James Lequeux*, EDP Sciences, 2003 Edited by J. Lequeux. *Astronomy and astrophysics library*, Berlin: Springer, 2005,
- Lin, C. C. & Shu, F. H. 1964, *ApJ*, 140, 646
- Lin, C. C. & Shu, F. H. 1966, *Proceedings of the National Academy of Science*, 55, 229
- Lindblad, B. 1927, *MNRAS*, 87, 420
- Liu, B., McIntyre, T., Terzian, Y., et al. 2013, *AJ*, 146, 80
- Lockman, F. J. 1979, *ApJ*, 232, 761
- Lockman, F. J. 1989, *ApJS*, 71, 469

- López-Corredoira, M., Hammersley, P. L., Garzón, F., et al. 2001, *A&A*, 373, 139
- Luna, A., Bronfman, L., Carrasco, L., & May, J. 2006, *ApJ*, 641, 938
- Martínez-García, E. E. & Puerari, I. 2014, *ApJ*, 790, 118
- Martínez-García, E. E., González-Lópezlira, R. A., & Bruzual-A, G. 2009, *ApJ*, 694, 512
- Mathewson, D. S., van der Kruit, P. C., & Brouw, W. N. 1972, *A&A*, 17, 468
- McClure-Griffiths, N. M., Dickey, J. M., Gaensler, B. M., et al. 2005, *ApJS*, 158, 178
- McClure-Griffiths, N. M., & Dickey, J. M. 2007, *ApJ*, 671, 427
- Mills, B. Y., Hill, E. R., & Slee, O. B. 1958, *The Observatory*, 78, 116
- Molinari, S., Swinyard, B., Bally, J., et al. 2010a, *A&A*, 518, L100
- Molinari, S., Swinyard, B., Bally, J., et al. 2010b, *PASP*, 122, 314
- Monguió, M., Grosbøl, P., & Figueras, F. 2015, *A&A*, 577, A142
- Nakanishi, H. & Sofue, Y. 2003, *PASJ*, 55, 191
- Nakanishi, H. & Sofue, Y. 2006, *PASJ*, 58, 847
- Olmi, L., Araya, E. D., Hofner, P., et al. 2014, *A&A*, 566, A18
- Oort, J. H., Kerr, F. J., & Westerhout, G. 1958, *MNRAS*, 118, 379
- Ortiz, R. & Lepine, J. R. D. 1993, *A&A*, 279, 90
- Pestalozzi, M. R., Minier, V., & Booth, R. S. 2005, *A&A*, 432, 737
- Peters, W. L., III 1975, *ApJ*, 195, 617
- Pettitt, A. R., Dobbs, C. L., Acreman, D. M., & Price, D. J. 2014, *MNRAS*, 444, 919
- Polido, P., Jablonski, F., & Lépine, J. R. D. 2013, *ApJ*, 778, 32
- Purcell, C. R., Longmore, S. N., Walsh, A. J., et al. 2012, *MNRAS*, 426, 1972
- Reid, M. J., Menten, K. M., Brunthaler, A., et al. 2014, *ApJ*, 783, 130
- Roberts, W. W. 1969, *ApJ*, 158, 123
- Robin, A. C., Luri, X., Reylé, C., et al. 2012, *A&A*, 543, AA100
- Robitaille, T. P., Churchwell, E., Benjamin, R. A., et al. 2012, *A&A*, 545, A39
- Rosolowsky, E., Dunham, M. K., Ginsburg, A., et al. 2010, *ApJS*, 188, 123
- Rots, A. H. 1975, *A&A*, 45, 43
- Russeil, D. 2003, *A&A*, 397, 133
- Sanders, D. B., Scoville, N. Z., & Solomon, P. M. 1985, *ApJ*, 289, 373
- Schönrich, R. 2012, *MNRAS*, 427, 274
- Sellwood, J. A. & Carlberg, R. G. 1984, *ApJ*, 282, 61
- Sevenster, M. N. 1999, *MNRAS*, 310, 629
- Shirley, Y. L., Ellsworth-Bowers, T. P., Svoboda, B., et al. 2013, *ApJS*, 209, 2
- Skrutskie, M. F., Cutri, R. M., Stiening, R., et al. 2006, *AJ*, 131, 1163
- Solomon, P. M., Sanders, D. B., & Rivolo, A. R. 1985, *ApJL*, 292, L19
- Stark, A. A. & Lee, Y. 2006, *ApJL*, 641, L113
- Steiman-Cameron, T. Y., Wolfire, M., & Hollenbach, D. 2010, *ApJ*, 722, 1460
- Stil, J. M., Taylor, A. R., Dickey, J. M., et al. 2006, *AJ*, 132, 1158
- Sun, Y., Xu, Y., Chen, X., et al. 2014, *A&A*, 563, A130
- Sun, Y., Xu, Y., Yang, J., et al. 2015, *ApJL*, 798, L27
- Tamburro, D., Rix, H.-W., Walter, F., et al. 2008, *AJ*, 136, 2872
- Thompson, M., Beuther, H., Dickinson, C., et al. 2014, *arXiv:1412.5554*
- Toomre, A. & Toomre, J. 1972, *ApJ*, 178, 623
- Vallée, J. P. 2008, *AJ*, 135, 1301
- Vallée, J. P. 2014a, *ApJS*, 215, 1
- Vallée, J. P. 2014b, *AJ*, 148, 5
- Vallée, J. P. 2015, *arXiv:1505.01202*
- van Woerden, H., Rougoor, G. W., & Oort, J. H. 1957, *Academie des Sciences Paris Comptes Rendus*, 244, 1691
- van der Kruit, P. C. 1971, *A&A*, 13, 405
- Velusamy, T., Langer, W. D., Goldsmith, P. F., & Pineda, J. L. 2015, *arxiv:1504.03373*
- Wada, K. 2008, *ApJ*, 675, 188
- Walsh, A. J., Breen, S. L., Britton, T., et al. 2011, *MNRAS*, 416, 1764
- Weaver, H. 1970, in *IAU Symposium*, Vol. 38, *The Spiral Structure of our Galaxy*, ed. W. Becker & G. I. Kontopoulos, 126
- Wright, E. L., Eisenhardt, P. R. M., Mainzer, A. K., et al. 2010, *AJ*, 140, 1868
- Xu, Y., Li, J. J., Hachisuka, K., et al. 2008, *A&A*, 485, 729
- Xu, Y., Li, J. J., Reid, M. J., et al. 2013, *ApJ*, 769, 15